ChemComm

COMMUNICATION

View Article Online
View Journal | View Issue

Cite this: *Chem. Commun.*, 2025, **61**, 9674

Received 8th April 2025,
Accepted 28th May 2025

DOI: 10.1039/d5cc01970b

rsc.li/chemcomm

Charge transfer alteration and white light emission in photochromic triphenylamine-norbornadiene-triazine switch†

Manoj Upadhyay, Raktim Deka and Debdas Ray *

Herein, we present a photochromic compound that reversibly switches emission colour by adjusting its charge transfer pathway. Its reversible photoisomerization toggles charge transfer through bonds or space, controlling white light emission. Computational and photophysical studies highlight its promise for advanced optoelectronic applications.

Photochromic molecules change form in response to external stimuli and have been widely studied for use in data storage,[1,2] optical switching,[3] energy storage,[4] and light-controlled electronics.[5] Researchers have explored well-known photoswitchable molecules like hydrazones,[6] diarylethenes,[7] spiropyrans,[8] fulgides,[9] and azobenzenes,[10] for their reliable and reversible transformations. The norbornadiene–quadricyclane (NBD–QC) couple stands out for solar energy storage,[4] molecular electronics,[11] and tunable photonics[2,12] due to its high-energy storage capacity, strong photostability, and rapid thermal reversibility. When NBD absorbs radiation, it undergoes an electrocyclic transformation to its metastable QC form, causing significant shifts in molecular geometry, conjugation, and electronic structure.[4,13] Over the past decade, researchers have developed donor–acceptor (D–A) systems for photovoltaics,[14] OLEDs,[15] bioimaging,[16] sensing, and nonlinear optics.[17] Controlling charge transfer (CT) in these systems is key to unlocking new applications.[18] Typically, in D–A systems, CT occurs *via* a through-bond charge transfer (TBCT) mechanism, where an extended π-system facilitates charge migration due to the delocalization of frontier molecular orbitals (FMOs).[19] However, studies show that through-space charge transfer (TSCT) can also occur *via* non-covalent interactions,[20] especially in systems with steric hindrance, non-conjugated linkers, or molecular twisting.[21] The ability to switch between TBCT and TSCT in a single molecule holds promise for developing multifunctional optoelectronic materials. To this context, designing white light emitters remains challenging due to the color balance.[6,22] Herein, we designed a donor–NBD–acceptor photochromic system that integrates a triphenylamine (TPA) donor and a triazine (TNZ) acceptor through a norbornadiene (NBD) bridge, forming **TPNTZ** (Fig. 1). The NBD/QC unit enables dynamic control of CT pathways under external light. In its initial NBD form, **TPNTZ** is expected to exhibit more prominent TBCT due to partial conjugation between TPA and TNZ. Upon photoisomerization to the QC isomer (**TPQTZ**), the molecular structure undergoes breaking of the conjugation, which leads to significant geometric distortion and increases the donor–acceptor separation. As a result, TBCT weakens while TSCT strengthens, leading to a shift in CT dynamics. UV-vis absorption analysis confirmed a reversible transformation between **TPNTZ** and **TPQTZ** with excellent fatigue resistance. Emission studies showed that **TPQTZ** emits blue light, while **TPNTZ** emits orange in methylcyclohexane (MCH) solution, revealing distinct CT characteristics. By adjusting **TPNTZ** and **TPQTZ** ratios by 365 nm light, we achieved white light emission. Quantum studies further validated the different extents of CT in **TPNTZ** and **TPQTZ**. This work provides fundamental insights into the tunable CT properties of donor–NBD/QC–acceptor systems modulated by photo-switching of the NBD/QC couple.

We synthesized **TPNTZ** using a one-step Suzuki coupling reaction,[23] where 2,3-dibromonorbornadiene was treated with (4-(diphenylamino)phenyl)boronic acid and 2,4-diphenyl-6-(4-(4,4,5,5-tetramethyl-1,3,2-dioxaborolan-2-yl)phenyl)-1,3,5-triazine simultaneously under an inert atmosphere (Scheme 1). After purification by column chromatography, the yellow solid formed with a 53% yield. NMR spectroscopy, mass spectrometry, and X-ray crystallography confirmed its structure (ESI†).

X-ray analysis showed that the triphenylamine donor and triphenyl-1,3,5-triazine acceptor attached to the NBD segment were out of plane, with torsion angles of −151.66° and −148.58°, when viewed along the C9–N8–C1–C2 and C1–N2–C26–C27 atoms, respectively (Fig. 1a and Fig. S3a and Table S1, ESI†). The donor and acceptor twisted slightly, forming an −18.64° angle. Adjacent phenyl rings created a 63.65° inter-plane angle (Fig. S3b, ESI†). As

Advanced Photofunctional Materials Laboratory, Department of Chemistry, Shiv Nadar Institution of Eminence, Delhi NCR, NH-91, Tehsil Dadri, Gautam Buddha Nagar, Greater Noida 201314, Uttar Pradesh, India. E-mail: debdas.ray@snu.edu.in

† Electronic supplementary information (ESI) available: Synthesis, characterization, SCXRD, computational analysis and PL studies. CCDC 2441493. For ESI and crystallographic data in CIF or other electronic format see DOI: https://doi.org/10.1039/d5cc01970b

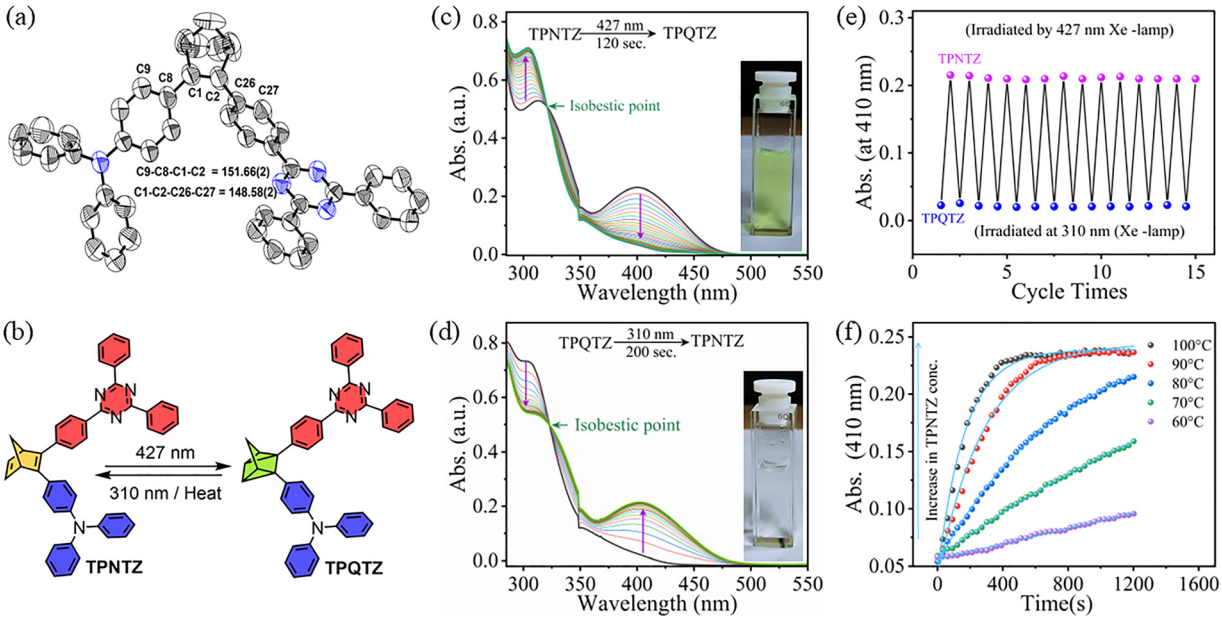

Fig. 1 (a) Oak Ridge thermal ellipsoid plots (50% probability ellipsoids) showing torsion angles. (b) Two-way photoswitching scheme of **TPNTZ** ⇆ **TPQTZ**. Absorption spectra in toluene showing photoisomerization of (c) **TPNTZ** → **TPQTZ** and (d) **TPQTZ** → **TPNTZ**. (e) Reversible switching in toluene under 427/310 nm light. (f) Kinetics plot of the thermal back-conversion from **TPQTZ** → **TPNTZ** in toluene at variable temperatures, monitored by the change in absorbance at 410 nm over time.

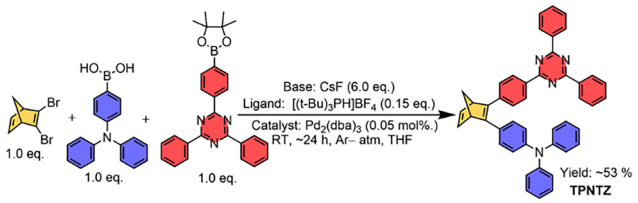

Scheme 1 Synthesis scheme of **TPNTZ**.

anticipated, the TNZ core stayed planar (0.127 Å deviation) and comparable to earlier reported crystals with similar molecular cores.[24] This planar conformation facilitates the formation of linear stacking of TNZ where π···π interactions (3.635 Å) occur between neighbouring triazine rings and adjacent phenyl rings (Fig. S3c, ESI†). Furthermore, as expected, all three phenyl groups of the TPA unit are angularly oriented to each other due to the free sp^3-hybridized nitrogen centre.

We studied the photochromic reaction of **TPNTZ**, tracking its conversion to the metastable **TPQTZ** form (Fig. 1b). Absorption measurement of **TPNTZ** in toluene revealed two distinct bands: one at 315 nm ($\varepsilon = 5.2 \times 10^4\ M^{-1}\ cm^{-1}$) and the other at 410 nm ($\varepsilon = 2.3 \times 10^4\ M^{-1}\ cm^{-1}$) (Fig. 1c). The higher-energy band resulted from a π–π* transition, while the lower-energy band reflected TBCT. When exposed to 427 nm blue light, the 360–500 nm absorbance gradually decreased and stabilized at 410 nm ($\varepsilon = 2.5 \times 10^3\ M^{-1}\ cm^{-1}$). Simultaneously, an increase was observed in the higher-energy band ($\varepsilon = 7.2 \times 10^4\ M^{-1}\ cm^{-1}$ at 310 nm), which leads to a colour change from green to transparent, indicating the gradual transformation of **TPNTZ** to **TPQTZ** over time (Fig. 1c). The isosbestic point at 322 nm indicated a well-defined, clean photoisomerization. Using first-order kinetics, we determined the isomerization rate constant in toluene to be $4.70 \times 10^{-2}\ s^{-1}$ under a photon flux of 3.9×10^{-9} mol s^{-1} (Fig. S4a, ESI†). To examine reverse photoisomerization, we irradiated **TPQTZ** in toluene with 310 nm UV light at its QC-centric absorption band. As **TPQTZ** converted back to **TPNTZ**, the higher-energy band started decreasing with an increase in lower-energy band intensity due to increased conjugation (Fig. 1d). Notably, there are only a few reports where QC-centric absorption activates back-isomerization.[25] The back photoisomerization rate constant in toluene was measured to be $2.79 \times 10^{-2}\ s^{-1}$ at a photon flux of 2.78×10^{-9} mol s^{-1} (Fig. S4b, ESI†). We calculated the photoisomerization quantum yields (ϕ) for both processes in various solvents (Fig. S4 and Table S2, ESI†). Notably, in toluene, $\phi_{(NBD \rightarrow QC)}$ reached 0.66 at 427 nm, while $\phi_{(QC \rightarrow NBD)}$ was 0.54 at 310 nm, demonstrating efficient reversible photoisomerization. To assess photostability, we irradiated **TPNTZ** solution (10 μM) with alternating 427 nm and 310 nm wavelengths for multiple cycles in toluene and MCH; monitoring absorbance at 410 nm leads to no significant change in absorbance, confirming high fatigue resistance (Fig. 1e and Fig. S5, ESI†). Although this couple shows excellent photoreversibility and high fatigue resistance in dilute solution, it undergoes photodegradation at higher concentrations which is common in NBD-derivatives (Fig. S6, ESI†).[11]

Furthermore, we explored charge transfer (CT) characteristics of the **TPNTZ**/**TPQTZ** couple in different solvents. **TPNTZ**'s absorption spectra remained largely unchanged across solvents of different polarities. **TPQTZ**, however, showed a redshift in its 350–450 nm low-energy tail and a hyperchromic increase in absorbance as the solvent polarity increased. This suggested that stronger dipole stabilization in polar solvents enhanced TSCT from the TPA donor

to the TNZ acceptor (Fig. S7, ESI†). We analyzed the thermal half-life ($t_{1/2}$) of **TPQTZ** at RT in toluene by examining its back conversion to **TPNTZ** in toluene at five different temperatures (Fig. 1f and Fig. S8, Table S3, ESI†).[26] From the Arrhenius plot, we estimated a $t_{1/2}$ of 56.5 hours at 298 K with an activation energy of 93.56 kJ mol^{-1}. The transition state entropy was calculated to be 41.66 J K^{-1} mol^{-1}, suggesting a moderate energy barrier and a concerted reaction mechanism with a well-ordered transition state. Importantly, the **TPNTZ/TPQTZ** switches demonstrated photothermal reversible (PTR) switching with outstanding fatigue resistance. Even after 20 cycles of irradiation and heating, the material consistently restored its absorbance, highlighting its robustness and thermal stability (Fig. S7c, ESI†). Interestingly, as the solvent polarity increases, the $t_{1/2}$ of the **TPQTZ**→**TPNTZ** thermal-back isomerization significantly decreases, suggesting that polar solvents assist CT from the donor to acceptor, facilitating the reverse isomerization (Fig. S9, ESI†).

We studied the emission of **TPNTZ** and **TPQTZ** in solvents with varying polarity. When excited at 410 nm, **TPNTZ** showed bright yellow-orange emission in MCH with an approximate photoluminescence quantum yield (ϕ_{PL}) of 83.4 ± 2%. As the polarity increased, emission shifted red and ϕ_{PL} dropped, confirming CT excited state stabilization (Fig. 2a and Table S3, ESI†). **TPQTZ**, excited at 310 nm, displayed a blue-shifted emission compared to **TPNTZ** (Fig. 2b). Importantly, in MCH, **TPQTZ** emitted a structured blue emission (ϕ_{PL} = 24.0 ± 3%), which became broad (red shifted) in polar solvents (Fig. 2b). This suggests that solvent polarity has a stronger effect on **TPQTZ**'s CT state than on **TPNTZ**. The measured ϕ_{PL} reflects both emissions, with each derivative dominating at different excitation wavelengths—410 nm and 310 nm. Earlier studies found that TSCT interactions respond more to solvent polarity than TBCT interactions.[27] **TPQTZ** facilitates TSCT because its TPA and TNZ units lack a direct conjugated bond. In contrast, **TPNTZ**'s TPA and TNZ units are covalently linked *via* an NBD bridge, promoting TBCT. This structural difference makes **TPQTZ** more sensitive to solvent polarity. **TPQTZ** shows higher ϕ_{PL} in polar solvents, suggesting solvent-driven CT from TPA to TNZ (Table S3, ESI†). Fluorescence decay studies revealed that both isomers had nanosecond decay times under aerated conditions, which increased with solvent polarity, indicating stabilization of the excited state (Fig. S10 and Table S4, ESI†). In MCH, **TPNTZ** emitted orange light at 565 nm, while **TPQTZ** emitted blue light at 445 nm (Fig. 2c). We aimed to produce white-light emission by balancing their concentrations. Absorption studies revealed that both **TPNTZ** and **TPQTZ** absorb weakly at 365 nm. Upon irradiation at this wavelength, photoisomerization of **TPNTZ** was initiated; however, a complete conversion to **TPQTZ** did not occur, leading to a photostationary state (PSS-365), with a **TPNTZ** fraction of 0.216 and with a **TPQTZ/TPNTZ** ratio of 3.6 : 1 (Fig. S11, ESI†). Exciting this at 365 nm resulted in white-light emission (ϕ_{PL} = 44.5 ± 2%), with Commission Internationale de l'Éclairage (CIE 1931) coordinates 0.335, 0.391 (Fig. 2c, d and Fig. S12, ESI†). Note that the total quantum yield (fluorescence and photoisomerization) exceeds 100% in MCH and toluene due to combined emission from the **TPNTZ/TPQTZ** isomeric pair.[12c,25] Moreover, photoswitching in the 5 wt% **TPNTZ**-polystyrene blend produced solution-like absorption changes and a visible, reversible color change (Fig S13, ESI†). Irradiation at 410 nm gradually reduced emission at 530 nm, suggesting decreased TBCT during isomerization to **TPQTZ**. Switching to 310 nm light restored the emission, confirming fully reversible photoswitching (Fig. S14, ESI†).

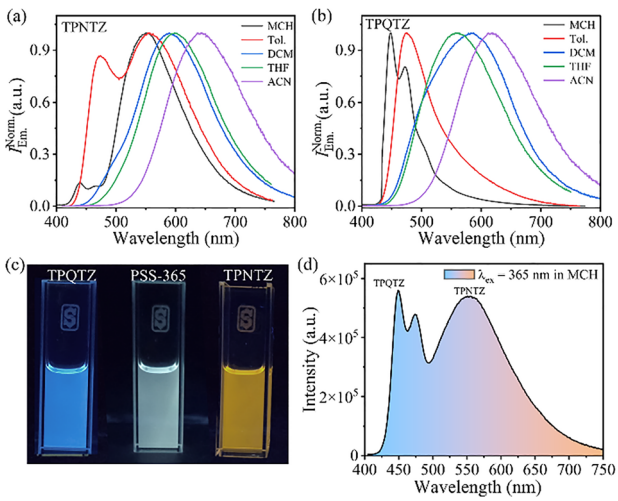

Fig. 2 PL spectra of (a) **TPNTZ** and (b) **TPQTZ** with solvents of disparate polarity. (c) Fluorescence photographs of **TPQTZ**, PSS-365, and **TPNTZ** under 365 nm UV-light in MCH. (d) Fluorescence spectra under 365 nm excitation in MCH.

We analyzed the electronic properties of **TPNTZ** and **TPQTZ** using density functional theory (DFT) and time-dependent DFT (TD-DFT) (ESI†).[28] In both isomers, FMOs were spatially separated with distinct localization patterns. In **TPNTZ**, the HOMO is largely localized on the TPA and double bond of NBD and extends somewhat over the first phenyl ring of the TNZ. The LUMO is mainly localized on the TNZ core, with minor contributions from the phenyl ring of TPA attached to the NBD. This significant HOMO–LUMO overlap results in a high oscillator strength (f = 0.5917) (Fig. S15a, ESI†). However, in **TPQTZ**, the HOMO is predominantly localized to TPA and the LUMO on the TNZ unit resulting in a comparatively low oscillator strength (f = 0.0064) (Fig. S15b, ESI†). Hole/electron analysis further revealed a contrasting result with **TPQTZ** showing a dominant CT character compared to its lower energy isomer owing to the well-separated hole and electron densities on the TPA and TNZ, respectively (Fig. 3a and b). This distinct separation weakens direct through bond interactions and enhances the possibility of TSCT). Further independent gradient model based on Hirshfeld partition of molecular density and inter-fragment charge transfer analyses at optimized S1 geometry confirmed the dominant TSCT (TPA → TNZ) character of **TPQTZ** (Fig. 3c).[29]

In summary, this study explored how structural changes in a photochromic donor–acceptor system control charge transfer. The system switches between through-bond and through-space charge transfer by breaking and reforming a C=C double bond. Photophysical analysis showed that controlled isomerization produces white-light emission, revealing new possibilities for optoelectronics.

D. R. acknowledges research funding from the Anusandhan National Research Foundation (ANRF) (ANRF/IRG/2024/000038/

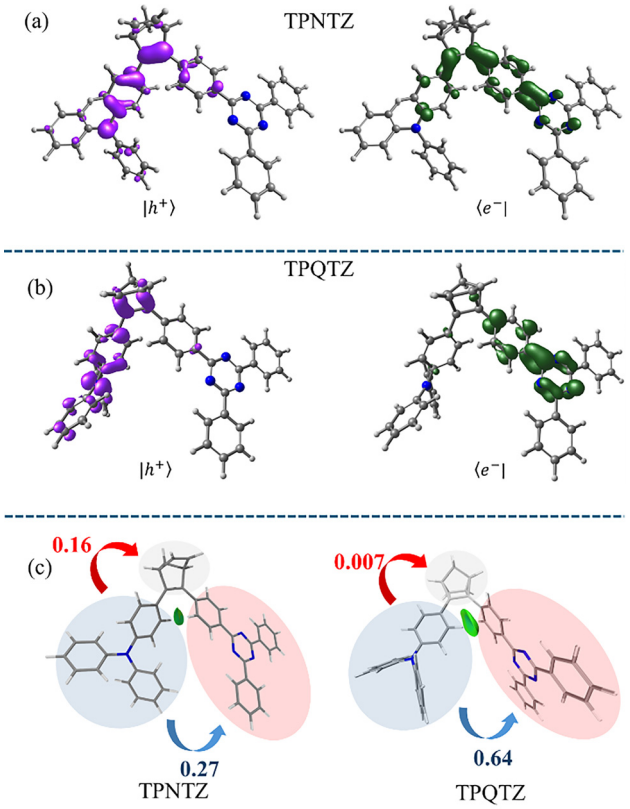

Fig. 3 (a) Hole–electron analysis (NTOs: |h+⟩, violet; ⟨e−|, green) for transition corresponding to the S1 and T1 excited states of (a) **TPNTZ** and (b) **TPQTZ** at isosurface values of ±0.002 a.u. [M06-2X/6-31g(d,p)]. (c) 3D visualization of non-covalent interaction and charge transfer amount in **TPNTZ** and **TPQTZ** (left to right); green isosurface refers to interactions.

CS), India and Science and Engineering Research Board (SERB) (CRG/2022/000128), Department of Science and Technology (DST), India. M. U. and R. D. thank SNIoE for their fellowships. The authors acknowledge the high-performance computing cluster 'MAGUS' at SNIoE for providing computational resources.

Data availability

The data supporting this article have been included as part of the ESI.†

Conflicts of interest

There are no conflicts to declare.

Notes and references

1 (*a*) S. Kawata and Y. Kawata, *Chem. Rev.*, 2000, **100**, 1777–1788; (*b*) V. Adam, H. Mizuno, A. Grichine, J.-I. Hotta, Y. Yamagata, B. Moeyaert, G. U. Nienhaus, A. Miyawaki, D. Bourgeois and J. Hofkens, *J. Biotechnol.*, 2010, **149**, 289–298.
2 W. Si, J. Li, G. Li, C. Jia and X. Guo, *J. Mater. Chem. C*, 2024, **12**, 751–764.
3 F. Höglsperger, B. E. Vos, A. D. Hofemeier, M. D. Seyfried, B. Stövesand, A. Alavizargar, L. Topp, A. Heuer, T. Betz and B. J. Ravoo, *Nat. Commun.*, 2023, **14**, 3760.
4 (*a*) A. Dreos, Z. Wang, J. Udmark, A. Ström, P. Erhart, K. Börjesson, M. B. Nielsen and K. Moth-Poulsen, *Adv. Energy Mater.*, 2018, **8**, 1703401; (*b*) R. R. Weber, C. N. Stindt, A. M. J. Harten and B. L. Feringa, *Chem. – Eur. J.*, 2024, **30**, e202400482.
5 (*a*) Z. Yang, P.-A. Cazade, J.-L. Lin, Z. Cao, N. Chen, D. Zhang, L. Duan, C. A. Nijhuis, D. Thompson and Y. Li, *Nat. Commun.*, 2023, **14**, 5639; (*b*) J. M. Mativetsky, G. Pace, M. Elbing, M. A. Rampi, M. Mayor and P. Samori, *J. Am. Chem. Soc.*, 2008, **130**, 9192–9193.
6 (*a*) B. Shao, N. Stankewitz, J. A. Morris, M. D. Liptak and I. Aprahamian, *Chem. Commun.*, 2019, **55**, 9551–9554; (*b*) M. D. Johnstone, C.-W. Hsu, N. Hochbaum, J. Andreasson and H. Sunden, *Chem. Commun.*, 2020, **56**, 988–991.
7 (*a*) T. Fukaminato, T. Hirose, T. Doi, M. Hazama, K. Matsuda and M. Irie, *J. Am. Chem. Soc.*, 2014, **136**, 17145–17154; (*b*) J. Zhang and H. Tian, *Adv. Opt. Mater.*, 2018, **6**, 1701278.
8 B. Seefeldt, R. Kasper, M. Beining, J. Mattay, J. Arden-Jacob, N. Kemnitzer, K. H. Drexhage, M. Heilemann and M. Sauer, *Photochem. Photobiol. Sci.*, 2010, **9**, 213–220.
9 Y. Yokoyama, *Chem. Rev.*, 2000, **100**, 1717–1740.
10 (*a*) H. D. Bandara and S. C. Burdette, *Chem. Soc. Rev.*, 2012, **41**, 1809–1825; (*b*) F. A. Jerca, V. V. Jerca and R. Hoogenboom, *Nat. Rev. Chem.*, 2022, **6**, 51–69.
11 E. E. Bonfantini and D. L. Officer, *Chem. Commun.*, 1994, 1445–1446.
12 (*a*) J. Ko, Y. Yoo, Y. Lee, H. Jeong and Y. Song, *iScience*, 2022, **25**, 104727; (*b*) M. Upadhyay, R. Deka and D. Ray, *J. Phys. Chem. Lett.*, 2024, **15**, 3191–3196; (*c*) B. E. Tebikachew, F. Edhborg, N. Kann, B. Albinsson and K. Moth-Poulsen, *Phys. Chem. Chem. Phys.*, 2018, **20**, 23195–23201; (*d*) S. Ghasemi, *et al.*, *Chem. – Eur. J.*, 2024, **30**, e202400322.
13 J. Orrego-Hernández, A. Dreos and K. Moth-Poulsen, *Acc. Chem. Res.*, 2020, **53**, 1478–1487.
14 (*a*) D. Zhang and M. Heeney, *Asian J. Org. Chem.*, 2020, **9**, 1251; (*b*) X. Wan, C. Li, M. Zhang and Y. Chen, *Chem. Soc. Rev.*, 2020, **49**, 2828–2842.
15 (*a*) S. Dey, M. Hasan, A. Shukla, N. Acharya, M. Upadhyay, S.-C. Lo, E. B. Namdas and D. Ray, *J. Phys. Chem. C*, 2022, **126**, 5649–5657; (*b*) H. Noda, X.-K. Chen, H. Nakanotani, T. Hosokai, M. Miyajima, N. Notsuka, Y. Kashima, J.-L. Brédas and C. Adachi, *Nat. Mater.*, 2019, **18**, 1084–1090.
16 (*a*) Z. Zhao, R. Du, X. Feng, Z. Wang, T. Wang, Z. Xie, H. Yuan, Y. Tan and H. Ou, *Curr. Med. Chem.*, 2025, **32**, 322–342; (*b*) S. Datta and J. Xu, *ACS Appl. Bio Mater.*, 2023, **6**, 4572–4585.
17 M. U. Khan, A. Fatima, S. Nadeem, F. Abbas and T. Ahamad, *Polycycl. Aromat. Compd.*, 2024, **44**, 5553–5583.
18 B. E. Tebikachew, H. B. Li, A. Pirrotta, K. Börjesson, G. C. Solomon, J. Hihath and K. Moth-Poulsen, *J. Phys. Chem. C*, 2017, **121**, 7094–7100.
19 S. Giannini and J. Blumberger, *Acc. Chem. Res.*, 2022, **55**, 819–830.
20 J.-T. Ye and Y.-Q. Qiu, *Phys. Chem. Chem. Phys.*, 2021, **23**, 15881–15898.
21 (*a*) S. Kumar, L. G. Franca, K. Stavrou, E. Crovini, D. B. Cordes, A. M. Slawin, A. P. Monkman and E. Zysman-Colman, *J. Phys. Chem. Lett.*, 2021, **12**, 2820–2830; (*b*) Y. Long, K. Chen, C. Li, W. Wang, J. Bian, Y. Li, S. Liu, Z. Chi, J. Xu and Y. Zhang, *J. Chem. Eng.*, 2023, **471**, 144759.
22 (*a*) S. Dey, R. Deka, M. Upadhyay, S. Peethambaran and D. Ray, *J. Phys. Chem. Lett.*, 2024, **15**, 3135–3141; (*b*) N. Acharya, M. Upadhyay, S. Dey and D. Ray, *J. Phys. Chem. C*, 2023, **127**, 7536–7545.
23 W. J. Yoo, G. C. Tsui and W. Tam, *Eur. J. Org. Chem.*, 2005, 1044–1051.
24 (*a*) S. Kumar, P. Rajamalli, D. B. Cordes, A. M. Slawin and E. Zysman-Colman, *Asian J. Org. Chem.*, 2020, **9**, 1277–1285; (*b*) H. Tanaka, K. Shizu, H. Nakanotani and C. Adachi, *Chem. Mater.*, 2013, **25**, 3766–3771.
25 L. Fei, H. Hölzel, Z. Wang, A. E. Hillers-Bendtsen, A. S. Aslam, M. Shamsabadi, J. Tan, K. V. Mikkelsen, C. Wang and K. Moth-Poulsen, *Chem. Sci.*, 2024, **15**, 18179–18186.
26 K. J. Laidler, *J. Chem. Educ.*, 1984, **61**, 494.
27 H. Tsujimoto, D.-G. Ha, G. Markopoulos, H. S. Chae, M. A. Baldo and T. M. Swager, *J. Am. Chem. Soc.*, 2017, **139**, 4894–4900.
28 M. J. Frisch, *et al.*, *Gaussian 16, Revision C.01. 2016*, Gaussian Inc., Wallingford, CT, 2016.
29 T. Lu and F. Chen, *J. Comput. Chem.*, 2012, **33**, 580–592.